Proceeding of the 9th International Symposium on Advanced Materials and Nanotechnology (iSAMN2025), October 29-30, 2025

Selective Growth and Characterization of Nanostructured Mo_6SnS_8 Chevrel Phase Thin Films: Structural, Optical, and Electrical Properties

S.M. **Aldosari**[1], Ftema W. **Aldbea***[2], A. **Boukhachem**[3]

[1] Innovation Parks, King Abdulaziz City for Science and Technology (KACST), Riyadh, 11442, Saudi Arabia
[2] Physics Department, Faculty of Science, Sebha University, Sebha, Libya
[3]Laboratory of Nanomaterials and Renewable Energy Systems, Research and Technology Center of Energy. Tunisia

* Corresponding author's phone: fte.aldbea@sebhau.edu.ly
Email: +218-911452162

Received: 01 October 2025; Accepted: 01 December 2025

ABSTRACT

The chevrel phase compound with the formula of $MnMo_6X_8$ is an important material that can be used for many applications, such as energy storage and electrocatalysis. Therefore, this work aims to produce Mo_6SnS_8 thin film using the spray pyrolysis technique and study its structural, optical, and electrical properties. The Mo6SnS8 ternary thin film has been prepared by the spray pyrolysis technique at a temperature of 250°C. Characterization via X-ray diffraction (XRD), spectrophotometry through reflectance and transmittance measurements, and electrical analysis via impedance spectroscopy were performed. X-ray analysis shows that the Mo6SnS8 material has a rhombohedral structure with a preferred orientation of the crystallites along the (110) direction parallel to the substrate plane. Optical measurements show a direct transition and energy gap of 3.60 eV. Electrical properties were measured using impedance spectroscopy technique over the frequency range 5 Hz–13 MHz at various temperatures. DC conductivity is thermally activated, showing a semiconductor behavior. A good semiconductor behavior observed for the $Mo6SnS_8$ film annealed at a low temperature.

Keywords— Thin film, spray pyrolysis, chevrel, semiconductor, XRD

1.0. INTRODUCTION

The chevrel phase with the formula of $M_xMo_6T_8$, where M is a metal; T = S, Se, or Te has received more attention because it exhibits a unique properties in science and technology fields [1]. Among the chevrel phase family, the molybdenum sulfide (Mo_6S_8) is one of the important compound where its crystal structure is related to $R\bar{3}$ space group with $a = b =$ 9.1833Å and c = 10.8716Å[2]. The Mo_6S_8 is considered an important material showing excellent physical and chemical properties. Therefore, it is a good candidate material to be suitable for energy storage, solar cells, and photocatalytic applications[1][3]. Many methods were used to prepare Mo_6S_8 material, such as sol- gel [4], hydrothermal [5], precipitation and spray pyrolysis [6]. In these methods, many elements were added to the Mo_6S_8 structure, such as Zn, Al, Cu, Mg, etc, in order to enhance its structural, optical and electrical properties [7][8][9]. Although many studies have been conducted on doped Mo_6S_8 with several elements, and they studied its physical and chemical properties, no study has been published about the spray pyrolysis of Mo_6SnS_8 thin film. In this work, the Mo_6SnS_8 thin film was prepared by using the spray pyrolysis and study its structural, optical and electrical properties

2.0. EXPERIMENTAL

The Mo_6SnS_8 thin film was deposited on a glass substrate at 250° C using 0.01 M of tin chloride hexahydrate ($SnCl_2$. $6H_2O$) and 610-2/7 M of Ammonium molybdate tetrahydrate [$(NH_4)_6Mo_7O_{24}.4H_2O$] and thiourea ($SC(NH_2)_2$, 20 10−2 M) aqueous solution. During the solution spraying, the nitrogen was used as carrier gas (pressure at 0.35 bar) through a 0.5 mm-diameter nozzle with a fixed nozzle-to-substrate plane distance of 27 cm and a flow rate was maintained at 4 mL/min. In addition, the substrate temperature was controlled by a thermocouple located on a metallic hot plate surface. After the deposition process, the coated substrate was kept cooling down naturally to room temperature.

2.1. Characterization

The structural measurements of the sample were performed using a Philips PW1710 X-ray diffractometer (XRD). This instrument uses CuKα radiation (λ = 0.154059 nm) and operates over a 2θ range between 10◦ and 70◦. The optical properties of the samples were measured using Schimadzu UV 3100 double-beam spectrophotometer, with the wavelength range of 300 - 2500 nm. The impedance measurements were recorded using the Hewlett–Packard HP4192 impedance analyzer. Where the real and imaginary components were measured at the temperature range of 295–355°C and in the frequency range (5 Hz–13 MHz).

3. RESULTS AND DISCUSSION

3.1 XRD analysis

Fig.1, shows the XRD pattern of Mo_6SnS_8 thin film. The sample has a single pure chevrel phase with the rhombohedral structure according to the JCPDS card no #01-08-1709[10]. The strong peak intensity due to enhance the crystallinity of the sample. Furthermore, the peak position is shifted to the right side which is a sign of the Sn incorporated into Mo_6SnS_8 structure[11]. The lattice parameters of the rhombohedral structure were determined using the unit cell software[12]. It is found that the lattice parameter values of Mo_6SnS_8 thin film were a= 9.466 Å and c= 10.736 Å. This value is close to the standard value of lattice parameters for pure Mo_6S_8 (a= 9.1833Å, and c= 10.8716Å) [13]. The cell volume value is about 833.205 $Å^3$. The large value of cell volume is attributed to the Sn entered into Mo_6S_8 structure.

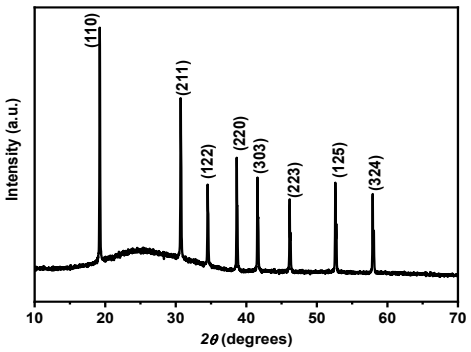

Fig.1: The XRD pattern of Mo_6SnS_8 thin film

3.2. Optical measurements

Fig. 2, shows the transmittance, reflectance and absorbance spectra of Mo_6SnS_8 thin film, which occurred below a wavelength value of 600 nm. It can be seen that, the sample showed transmittance, reflectance and absorbance values of ~ 16%, 15%, and 70%, respectively. The high absorbance value indicates that the sample is suitable for photocatalytic applications.

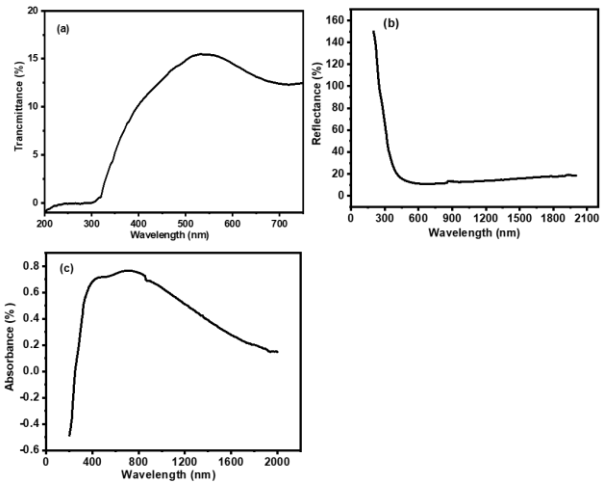

Fig 2: (a) transmittance, (b) reflectance and (c absorbance of Mo_6SnS_8 thin film

The absorption coefficient (α) is estimated from absorbance spectra using the formula[14]:

$$\alpha(\lambda) = ln\frac{(1-R(\lambda))^2}{T(\lambda)} \quad (1)$$

where R is the reflectance and T is the transmittance. The value of α was in the range of 10^6 cm^{-1} (Fig 3a), which is the same range as strong semiconductor materials with the direct band gap (α between 10^4- 10^6 cm^{-1})[15].

The energy gap (E_g) of the thin film was estimated using the formula[16]:

$$(\alpha h\nu) = A(h\nu - E_g)^n \quad (2)$$

where n has two values, $\frac{1}{2}$ for direct and n=1 for indirect energy gap, h is Planck's constant, and ν is the frequency. The Mo_6SnS_8 thin film has a direct E_g. Therefore, to determine the E_g value, the transition is allowed to find the best fit for the extrapolation for the x- axis. Then, the direct E_g value was estimated from the Tauc plot of $(\alpha h\nu)^2$ versus $h\nu$ (see Fig 3b). From the Figure it, can be seen that the sample has an energy gap value of about 3.60 eV, which is higher than 1.76 eV for $Ni_2Mo_6S_8$ [9]. The optical properties of the chevrel phase are still under investigation.

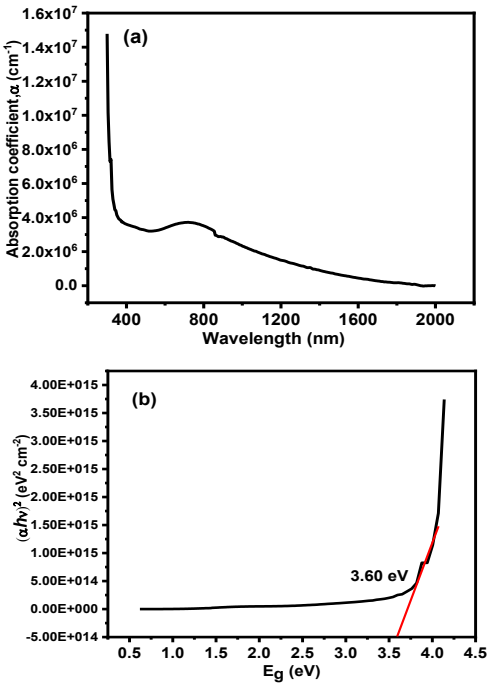

Fig 3: (a) absorption coefficient and (b) energy gap of Mo_6SnS_8 thin film

3.3. Electrical analysis

Fig 4 , shows the impedance analysis of the Mo_6SnS_8 thin film at the temperature ranges from 295 to 355 °C. Fig 4a shows the imaginary part (Z´´) against real part (Z´) (Nyquist plot). From the Figure, it can be seen that the semi-circles are shifted to the low frequency as the temperature is increased to 355°C due to a small contribution from impedance equipment[17]. Also, the single arc indicates that relaxation process occurred in the film; in this case, the parallel RC circuit was used [18]. Furthermore, the decrease in the semi-circles` diameters with increased temperature is a sign to enhance the electrical conductivity and the reduction in the bulk resistance [19]. The variation of the Z´´ with the frequency of the film at different temperatures is illustrated in Fig 4b. A high relaxation peak of the film appeared at a low temperature value of 295 °C. Then, this peak is decreased with increased the temperature, and it shifted to the higher frequency value, which referred to the thermal activation of local charge carriers and a temperature-dependent relaxation time[6].

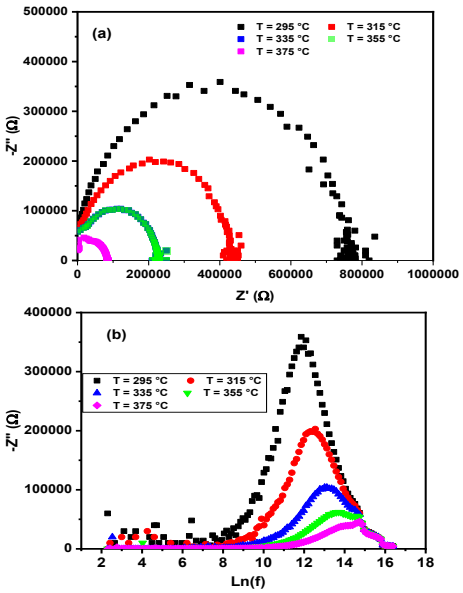

Fig 4: (a) variation of the real and imaginary parts (b) variation of imaginary component with the frequency at different temperature of Mo_6SnS_8 thin film

Fig. 5, shows the relation between ionic conductivity (ln σ) and the temperature (1000/T). The results show a linear drop and the regression value (R^2) of 0.99 near to unity, which matches with the Arrhenius law (Eq(3)[20]:

$$\sigma = \sigma_0 \exp\left(\frac{-E_a}{k_B T}\right) \quad (3)$$

Where σ is the ionic conductivity, σ_0 is the exponential factor, E_a is the activation energy (eV), k_B is the Boltzmann constant (8.617 x10^{-5} eV/K) and T is the absolute temperature (K).

The value of E_a was found to be about 0.88 eV, which means the ionic mobility is poor at lower temperatures as this value indicates the semiconductor behavior with a high activation energy[20][21].

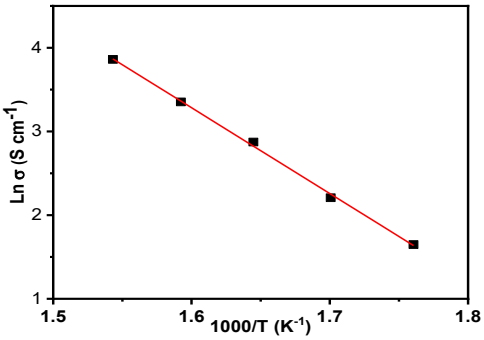

Fig 5: the relation between ionic conductivity (ln σ) and the temperature (1000/T)

The variation of ln (σ) against ln (f) (f was selected from 3 Hz to 13MHz) at different temperatures is shown in the Fig 6, where σ is the measured conductivity, which contains two terms, dc and ac conductivities, according to the following formula[22]:

$$\sigma = \sigma_{ac} + \sigma_{dc} \quad (4)$$

At low frequency values, σ is approximately independent; this might be related to the σ_{dc} contribution[22]. The conductivity observed to increase linearly in the higher frequency range. The mechanism of this behavior can be explained by correlated barrier hopping (CBH) model, where the ions mostly transfer through a material by hopping between sites. The hopping probability between nearby sites is correlated, resulting in a frequency-dependent AC conductivity[23].

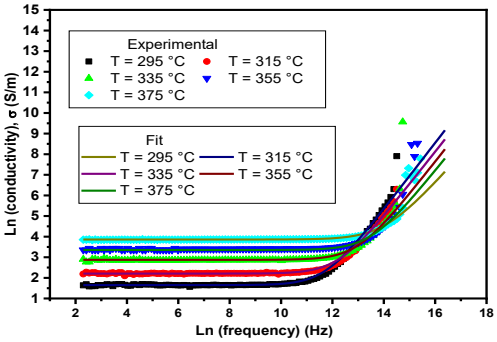

Fig 6: the plot of ln(σt) versus ln(f) at different temperatures for Mo_6SnS_8 thin film

Fig.7, illustrates the variation of the exponent s with the temperature. The s value was determined from the slope of logarithmic conductivity against frequency (it is not shown in this work). It can be seen that, the value of s decreased with the temperature. This gives an idea that the charge is being bound in traps-like manner[19]. The value of s is recorded to be -0.003, which is smaller than the value of the energy gap (weak charge bond). This result is reasonable due to the increase in conductivity[21].

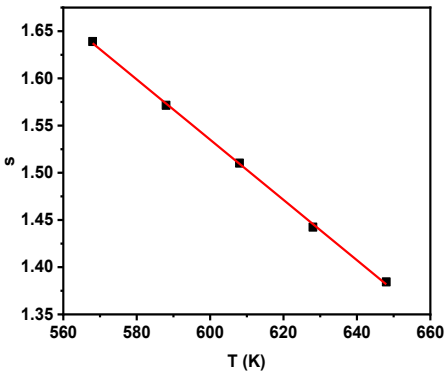

Fig 7: the plot of s versus T for Mo_6SnS_8 thin film

4.0 CONCLUSIONS

The Mo_6SnS_8 thin film was prepared using the spray pyrolysis technique at a temperature of 250 °C. The film has a

rhombohedral crystal structure with a preferred orientation of the crystallites along the (110) plane. The optical measurement of the thin film exhibits a strong absorption spectrum and a high direct energy gap. The electrical properties of the film illustrated a high activation energy and a strong semiconductor behavior. This unusual behavior will be investigated in the Future work

REFERENCES

[1] M. Liu *et al.*, "Chevrel phase: A review of its crystal structure and electrochemical properties," *Prog. Nat. Sci. Mater. Int.*, vol. 33, no. 1, pp. 8–15, 2023, doi: https://doi.org/10.1016/j.pnsc.2023.01.002.

[2] L. Geng, J. P. Scheifers, J. Zhang, K. N. Bozhilov, B. P. T. Fokwa, and J. Guo, "Crystal Structure Transformation in Chevrel Phase Mo6S8 Induced by Aluminum Intercalation," *Chem. Mater.*, vol. 30, no. 23, pp. 8420–8425, Dec. 2018, doi: 10.1021/acs.chemmater.8b03312.

[3] M. L. Agiorgousis, Y. Sun, D. J. West, and S. Zhang, "Material for Energy Generation and Storage Intercalated Chevrel Phase Mo 6 S 8 as a Janus Material for Energy Generation and Storage," 2018, doi: 10.1021/acsaem.7b00092.

[4] S. Boursicot, V. Bouquet, I. Péron, T. Guizouarn, M. Potel, and M. Guilloux-Viry, "ChemInform Abstract: Synthesis of Cu2Mo6S8 Powders and Thin Films from Intermediate Oxides Prepared by Polymeric Precursor Method.," *Solid State Sci.*, vol. 14, pp. 719–724, Jun. 2012, doi: 10.1016/j.solidstatesciences.2012.03.013.

[5] X. Xu, M. Zhang, J. Wu, Z. Shen, Y. Liu, and L. Wang, "Advanced Progress of Non-Stoichiometric Transition Metal Sulfides for Sensing, Catalysis, and Energy Storage," *Nanomaterials*, vol. 15, no. 16, p. 1237, 2025.

[6] P. Saha, P. H. Jampani, M. K. Datta, C. U. Okoli, A. Manivannan, and P. N. Kumta, " A Convenient Approach to Mo 6 S 8 Chevrel Phase Cathode for Rechargeable Magnesium Battery ," *J. Electrochem. Soc.*, vol. 161, no. 4, pp. A593–A598, 2014, doi: 10.1149/2.061404jes.

[7] P. Yu *et al.*, "The evolution of local structure of Mo6S8 during Li+ electrochemical storage studied by in-situ tender X-ray absorption spectroscopy," *Prog. Nat. Sci. Mater. Int.*, vol. 32, no. 6, pp. 739–744, 2022, doi: https://doi.org/10.1016/j.pnsc.2022.09.006.

[8] X. Qi *et al.*, "Surface Optimization of Mg Metal Electrodes by Tuning Pilling–Bedworth Ratio for Long-Life Mg Batteries," *Renewables*, vol. 3, no. 2, pp. 77–86, 2025, doi: 10.31635/renewables.025.20250008 1.

[9] M. Pawar, A. Annerino, J. Shell, and P.-I. Gouma, "Photocatalytic Desulfurization of Thiophene with Chevrel Phase Ni2Mo6S8 Synthesized by SHS," *ACS Omega*, vol. 9, no. 31, pp. 33935–33940, Aug. 2024, doi: 10.1021/acsomega.4c04213.

[10] K. M. Naik and S. Sampath, "Cubic Mo6S8-Efficient Electrocatalyst Towards Hydrogen Evolution Over Wide pH Range," *Electrochim. Acta*, vol. 252, pp. 408–415, 2017, doi: https://doi.org/10.1016/j.electacta.2017.09.015.

[11] F. W. Aldbea, N. B. Ibrahim, and M. Yahya, "Effect of adding aluminum ion on the structural, optical, electrical and magnetic properties of terbium doped yttrium iron garnet nanoparticles films prepared by sol-gel method," *Appl. Surf. Sci.*, vol. 321, 2014, doi: 10.1016/j.apsusc.2014.10.019.

[12] T. J. B. Holland and S. A. T. Redfern, "Unit cell refinement from powder diffraction data: the use of regression diagnostics," *Mineral. Mag.*, vol. 61, no. 404, pp. 65–77, 1997, doi: DOI: 10.1180/minmag.1997.061.404.07.

[13] M. S. Chae, J. W. Heo, S.-C. Lim, and S.-T. Hong, "Electrochemical Zinc-Ion Intercalation Properties and Crystal Structures of ZnMo6S8 and Zn2Mo6S8 Chevrel Phases in Aqueous Electrolytes," *Inorg. Chem.*, vol. 55, no. 7, pp. 3294–3301, Apr. 2016, doi: 10.1021/acs.inorgchem.5b02362.

[14] M. Allaham *et al.*, "Energy gap measurements based on enhanced absorption coefficient calculation from transmittance and reflectance raw data," *Phys. Scr.*, vol. 99, no. 2, pp. 1–9, 2024, doi: 10.1088/1402-4896/ad1cb8.

[15] H. J. Lee, M. M. A. Gamel, P. J. Ker, M. Z. Jamaludin, Y. H. Wong, and J. P. R. David, "Absorption Coefficient of Bulk III-V Semiconductor Materials: A Review on Methods, Properties and Future Prospects," *J. Electron. Mater.*, vol. 51, no. 11, pp. 6082–6107, 2022, doi: 10.1007/s11664-022-09846-7.

[16] H. H. Kusuma, M. K. Saidin, and Z. Ibrahim, "Optical properties of Ti: Al2O3 single crystal," *J. Fiz. UTM*, vol. 4, pp. 42–49, 2009.

[17] A. Huanosta, J. C. Alonso, and A. Ortiz, "Spectroscopic impedance studies of Al2O3 films deposited by spray pyrolysis," *Thin Solid Films*, vol. 401, no. 1, pp. 284–290, 2001, doi: https://doi.org/10.1016/S0040-6090(01)01621-2.

[18] A. Manan, G. S. Jahan, M. U. Rehman, and M. T. Lanagan, "Synthesis, dielectric and impedance spectroscopy study of temperature stable Ta2O5 modified 0.85BaTiO3-0.15Bi(Mg0.5Ti0.5)O3 ceramics," *Chem. Phys. Impact*, vol. 7, p. 100376, 2023, doi: https://doi.org/10.1016/j.chphi.2023.100376.

[19] M. N. Hafiza and M. I. N. Isa, "Conduction mechanism via correlated barrier hopping in EC-plasticized 2-hydroxyehyl cellulose-ammonium nitrate solid polymer electrolyte," *IOP Conf. Ser. Mater. Sci. Eng.*, vol. 440, no. 1, 2018, doi: 10.1088/1757-899X/440/1/012039.

[20] N. Kumar, S. K. Patri, and R. N. P. Choudhary, "Frequency-temperature response of a new multiferroic," *Process. Appl. Ceram.*, vol. 8, no. 3, pp. 121–125, 2014, doi: 10.2298/PAC1403121K.

[21] R. M. Rudenko, O. O. Voitsihovska, and V. N. Poroshin, "Sequential change of semiconductor mechanisms of electrical conductivity in ternary PVDF/polyaniline/MWCNT nanocomposite in the wide temperature range of 4.2–340 K," *Mater. Lett.*, vol. 350, p. 134976, 2023, doi: https://doi.org/10.1016/j.matlet.2023.134976.

[22] M. Jebli, C. Rayssi, J. Dhahri, and K. Khirouni, "Investigation of electrical properties and conduction mechanism using CBH model of

Ba0.97La0.02Ti1−xNb4x/5O3 (x = 0.00 and 0.02) compounds," *Appl. Phys. A*, vol. 126, no. 2, p. 109, 2020, doi: 10.1007/s00339-020-3298-x.

[23] P. Dhuria, S. S. Bhamra, and J. S. Hundal, "The study of Correlated Barrier Hopping (CBH) conduction mechanism and modulus spectroscopy of YFe0.5Co0.5O3 compound," *Phys. B Condens. Matter*, vol. 677, p. 415696, 2024, doi: https://doi.org/10.1016/j.physb.2024.415696.